nature geoscience

Article

https://doi.org/10.1038/s41561-025-01842-w

Westerly wind shifts drove Southern Hemisphere mid-latitude peat growth since the last glacial

Received: 7 June 2024

Accepted: 3 October 2025

Published online: 11 November 2025

Check for updates

Zoë A. Thomas[1] ✉, Haidee Cadd[2], Chris Turney[3,4], Lorena Becerra-Valdivia[5,6], Heather A. Haines[7], Chris Marjo[8], Christopher Fogwill[9], Stefanie Carter[10,11] & Paul Brickle[10,12]

Extratropical peatlands in the Southern Hemisphere preserve detailed information on climatic and environmental change going back millennia. They are particularly valuable for understanding the evolution of the mid-latitude southern westerly winds (SWW), which play a major role in driving regional temperature and precipitation patterns, Antarctic sea-ice extent and ocean carbon fluxes. Here we investigate the timing and drivers of peatland initiation across the southern mid-latitudes after the Last Glacial Maximum (21,000 years ago) and test how this might relate to past changes in the SWW. We radiocarbon-date basal peats from the Falkland Islands and collate published basal peat radiocarbon ages from peat-forming regions south of 35° S. Using kernel density estimate models, we find distinct latitudinal phases of post-glacial peat initiation that suggest that peat growth is sensitive to variations in SWW position through their influence on moisture availability, temperature and dust deposition. A peak in peat growth in regions north of 52.5° S during the Antarctic Cold Reversal (14,700–12,800 years ago) suggests an equatorward migration of the SWW, coinciding with a slowdown in atmospheric CO_2 increases. In light of recent SWW intensification and poleward migration, our findings highlight the potential for ongoing changes in the Southern Hemisphere climate and carbon fluxes under continued anthropogenic heating.

The southern mid-latitudes are critical for understanding past global environmental change and anticipating future human-driven climate impacts[1]. Situated between the tropics and the pole, this region provides unique insights into the behaviour of the southern westerly winds (SWW); phenomena that drive hemispheric-wide changes including regional temperature and precipitation extremes and trends, sea-ice dynamics, Antarctic Ice Sheet mass balance and air–ocean CO_2 exchange[2–5]. This circumpolar belt of westerly airflow spans roughly 40° S to 60° S through the year, with its core flow currently centred around 52° S (ref. 6) (Fig. 1). Precisely characterizing spatial and temporal SWW variability remains challenging because proxy records are sparse, unevenly distributed in latitude or lack sufficient sampling resolution and chronological control[7]. Peat deposits from southern South America, New Zealand, Tasmania and sub-Antarctic islands preserve highly detailed climate and environmental records across the mid- to high latitudes[8–12], offering valuable insights into the drivers of climate variability and their impacts. Inferring latitudinal shifts in the SWW has proved challenging, however, as although many proxies can provide high-resolution reconstructions of past wind strength[13–21], individual records cannot indicate past wind latitudes,

A full list of affiliations appears at the end of the paper. ✉e-mail: z.thomas@soton.ac.uk

and most are limited in length to the Holocene. In this study we use the onset of peat initiation across a network of sites spanning the southern mid-latitudes as a climate-sensitive proxy to reconstruct SWW changes during key climatic transitions.

The last deglaciation (~19,000–11,700 cal. yr BP (calibrated years before present, where present = 1950 CE) was a pivotal phase in Earth's climate history, marked by a gradual warming trend interrupted by rapid and opposing climate shifts between the northern and southern mid- to high latitudes[22]. In the Southern Hemisphere, deglacial warming was accompanied by glacier retreat, Antarctic sea-ice decline and rising atmospheric CO_2 and sea levels. However, this trend was interrupted by the Antarctic Cold Reversal (ACR), an ~2,000-year-long period starting around 14,700 cal. yr BP when cold conditions returned and atmospheric CO_2 plateaued, before deglacial warming and CO_2 rise resumed. These changes were closely tied to movements in the SWW, although their precise latitudinal shifts remain uncertain.

Drivers of peat initiation

There are several pathways to peatland initiation, but the most common in the southern mid-latitudes is primary peat formation, where peat accumulates directly on water-saturated mineral clay (often of glacial/periglacial origin)[9]. Other pathways include terrestrialization (the infilling of limnic systems with organic matter) and paludification (the formation of peat due to a rise in the water table)[23]. On decadal to millennial timescales, temperature and moisture availability are considered the most important drivers of peat formation[24]. However, disentangling the relative influences of temperature and precipitation changes on local and regional hydrology and moisture balances, as well as vegetation composition, is complex[25–27]. Local factors such as microtopography[28], isostatic adjustments and opportunities for colonization in areas newly exposed by retreating glaciers also influence peat growth. In general, warmer climates with sufficient precipitation will result in longer growing seasons for vegetation, enhance plant productivity and promote peat and carbon accumulation[29].

Distinct phases of peat formation

Here we present new basal peat dates from the Falkland Islands (Supplementary Data 1; ref. 30) doubling the available data from this region. We also compile published basal peat ages from across the southern mid-latitudes, creating a dataset that contains 237 basal ages from 201 sites (Fig. 1; see also Supplementary Data 1, ref. 30 and Supplementary Figs. 2–7). All new and previously published basal ages were recalibrated with the latest Southern Hemisphere radiocarbon calibration curve (SHCal20; ref. 31). To investigate the spatial and temporal phases of peat initiation we applied kernel density estimate (KDE) modelling and summed probability distributions across regional sectors and latitudinal bands. These phases are compared with independent climate proxy records to place the timing of peat initiation in the context of broader mid-latitude climatic changes.

We identify several phases of peat initiation across the southern mid-latitudes during the last deglaciation and Holocene (Fig. 2). Peat growth in this region began by ~20,000 cal. yr BP, several thousand years earlier than widespread peat establishment in the Northern Hemisphere (11,000 cal. yr BP)[27]. The first major peak in peat initiation at 16,000 cal. yr BP is dominated by sites in the highest latitudinal band (52.5–55° S; Fig. 2a), consistent with an inferred poleward position of the SWW reconstructed from marine records[32]. This poleward shift would have resulted in the advection of warmer airmasses over these latitudes and coincided with the deglaciation of the Patagonian Ice Sheet[33].

The highest density of peat initiation across most latitudinal bands, however, is centred on 14,000–13,000 cal. yr BP (Fig. 2). This contrasts with earlier large data compilations[27], which noted a 'gap' in peat initiation ages, interpreted as a pause in peat initiation during the cooler temperatures associated with the ACR. However, our expanded

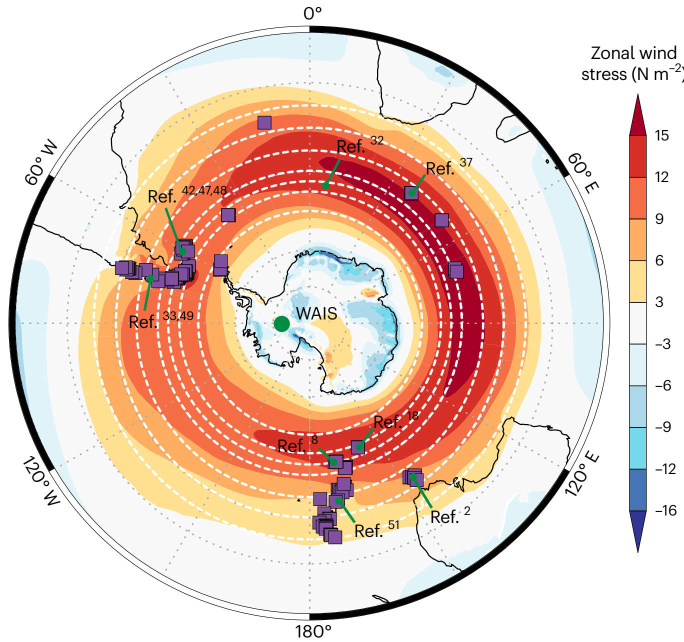

Fig. 1 | Zonal winds and study site locations. Zonal wind stress at 850 hPa (averaged 2015–2020) from European Reanalysis ERA5[64], with the locations of basal peat sites indicated by purple squares (not all sites are distinguishable due to overlap). White dashed lines indicate the latitudinal boundaries (35° S, 40° S, 45° S, 50° S, 52.5° S, 55° S and 60° S). The locations of selected proxy records discussed in the text are indicated by the green circles: Anderson et al.[32]; Nel et al.[37]; Saunders et al.[18]; Fletcher et al.[2]; McGlone et al.[8]; Tielidze et al.[51]; Davies et al.[33]; Moreno et al.[49]; Monteath et al.[42]; Spoth et al.[48]; Scaife et al.[47], WAIS; West Antarctic Ice Sheet Divide Core[65].

dataset shows that this apparent gap is only associated with the highest latitudinal band (52.5–55° S), where the KDE reveals a prominent dip, implying that the southernmost range of SWW airflow migrated to the north at this time. In contrast, the 50–52.5° S and 45–50° S latitudinal bands both peak at 13,000 cal. yr BP, indicating that conditions there remained favourable for peat growth despite the temperature decrease associated with the ACR. Peat initiation in the southernmost latitudinal band of 52.5–55° S increases again at 11,000 cal. yr BP, while the more northward latitudinal bands decline, suggesting a post-ACR southward shift of the SWW. Clusters of basal peat ages across South America, the South Atlantic and the Southwest Pacific indicate that this latitudinal pattern holds across the Southern Hemisphere, regardless of longitude (except in the South Indian Ocean sector, where all sites fall within 45–50° S; Supplementary Table 1).

During the Holocene, peat initiation increases in the 45–52.5° S bands between 8,000 and 7,000 cal. yr BP, before declining across all bands. By this time, it is likely that most suitable peat-forming landscapes had begun to accumulate peat, and that accommodation space for peat growth was largely filled. Subsequent small peaks probably reflect local factors.

Interpretation of basal peat data

The strength and latitudinal position of the SWW directly influence the intensity of zonal atmospheric flow and play a crucial role in shaping precipitation patterns across the Southern Ocean region. Extratropical precipitation is primarily generated by frontal systems associated with surface depressions that develop in direct response to variations of the upper-level westerly winds. Stronger westerlies enhance the growth of these depressions, driving more frequent and intense storm activity that contributes to increased precipitation and the advection of warm airmasses polewards[34,35]. Consequently, intensified westerlies at inter-annual and longer timescales result in a higher frequency and intensity

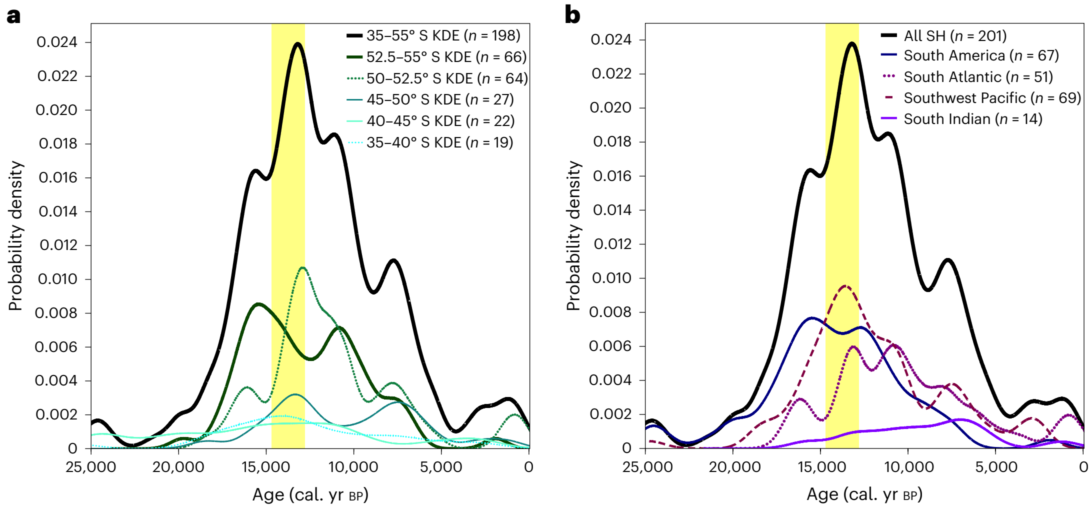

Fig. 2 | Patterns in Southern Hemisphere peat initiation. a,**b**, KDEs of peat initiation by latitude (**a**) and sector (**b**). The yellow bands denote the ACR (14,700–12,800 cal. yr BP). Note that there are three sites south of 55° S, which explains the discrepancy between all Southern Hemisphere (SH) sites (n = 201) and 35–55° S (n = 198).

of extratropical storms, leading to greater precipitation and warming across the southern mid-latitudes. Sub-Antarctic islands located within the mid-latitude storm track are strongly influenced by passing frontal systems and exhibit a positive correlation between zonal wind speed and precipitation (Supplementary Fig. 8). However, this relationship can be modulated by local topography: orographic uplift enhances rainfall on the windward side of mountain ranges (for example, the Patagonian Andes, New Zealand's Southern Alps and Tasmania's west coast), while the leeward slopes experience drier conditions due to downslope subsidence and increased evaporation. Such west–east precipitation gradients complicate interpretation of the link between stronger SWW and moisture conditions conducive to peat growth[2,34].

Beyond direct precipitation influences, other factors indirectly linked to the SWW also affect water availability. Glacier meltwater streams probably supported some peatlands[36] and variations in SWW strength may have influenced glacial dynamics by altering temperature and precipitation patterns, thereby affecting meltwater availability and indirectly contributing to peatland initiation and growth. Sea-ice expansion associated with a northward shift in the SWW would also have been important in limiting moisture availability by reducing oceanic evaporation and inhibiting the formation of precipitation-bearing weather systems[37]. This would have had a pronounced effect on sub-Antarctic islands, potentially constraining peatland formation during the ACR[37]. Another potential mechanism linking the SWW and peat formation is nutrient transport via wind-blown dust that enhances ecosystem productivity and promotes peat accumulation[38]. For instance, short-lived increases in carbon accumulation have been observed in peat bogs following tephra deposition in New Zealand[39], indicating that external nutrient inputs can influence peat growth. However, while dust deposition may stimulate productivity, a connection between dust-derived nutrients and peatland initiation has not been directly demonstrated.

There are other factors unrelated to westerly wind shifts that can be locally important in the initiation of peatlands. Large areas of Patagonia, some areas of New Zealand and some sub-Antarctic islands were glaciated during the Last Glacial Maximum, preventing peat formation in these areas. Although basal peat dates have sometimes been used to infer the timing of deglaciation, many studies report lags of several thousand years between glacier retreat and peat establishment[26,37], indicating that the timing of glacier retreat is not a major determinant of peat initiation after 16,000 cal. yr BP. Other local geomorphological factors, such as bedrock type, probably did influence peat formation in certain locations. On Marion Island, for example, peatlands underlain by black lavas have younger basal dates than those on other substrates, probably due to unfavourable conditions for paludification[37]. Similarly, volcanic activity that disrupted natural drainage patterns may have delayed peat initiation in some regions.

Sea-level rise during deglaciation presents another potential, but limited, influence. While some coastal peatlands may have been gradually inundated, most were farther inland at their point of initiation. A relative elevation change of over 100 m (ref. 40) would have corresponded to a gradual increase in mean air temperature of ~1 °C, but it is unlikely that this modest warming over several thousand years would have played a key role in peat formation. The widespread presence of peat on all sub-Antarctic islands and continental landmasses well before the Holocene sea-level high stand indicates that sea-level rise was not a major factor influencing peat initiation during the deglaciation.

Extreme and abrupt changes in SWW during the deglaciation and Holocene

We show that latitudinal patterns of peat initiation provide a valuable proxy for tracking the migration of the SWW through the deglaciation and early Holocene (Fig. 3). This is particularly evident during the ACR, where cooling over Antarctica (reflected in a decrease in ice core $\delta^{18}O$; Fig. 3d), a plateau in global CO_2 (Fig. 3e) and sea-ice expansion[41] are inferred to have driven a northward shift in the SWW[2,42]. These changes occur simultaneously with reduced peatland initiation in the southernmost latitudinal band (52.5–55° S), and a peak in the 52.5–50° S band, consistent with our interpretation that a strong presence of the westerly winds promoted peat initiation, and that the southern limit of the SWW migrated northwards of 52.5° S at this time. After the ACR, this pattern reverses, with peat growth in the southernmost latitudinal band (52.5–55° S) peaking at ~11,000 cal. yr BP, suggesting a shift of the SWW to a more poleward position (Fig. 4).

Our analysis assumes zonal symmetry of the SWW during the deglaciation; this assumption is supported by terrestrial hydroclimate reconstructions that show broadly synchronous, multimillennial moisture trends linked to the SWW between 15,000 and 5,000 cal. yr BP[43]. Over the past 5,000 years, the increased influence of the El Niño/Southern Oscillation and its teleconnections has resulted in the apparent loss of zonal symmetry[44,45]. We acknowledge that due to the spatial distribution of landmasses, our dataset is weighted towards the Atlantic and Pacific sectors and our interpretations are most robust for these regions (Supplementary Table 1). In addition, we do not

https://doi.org/10.1038/s41561-025-01842-w

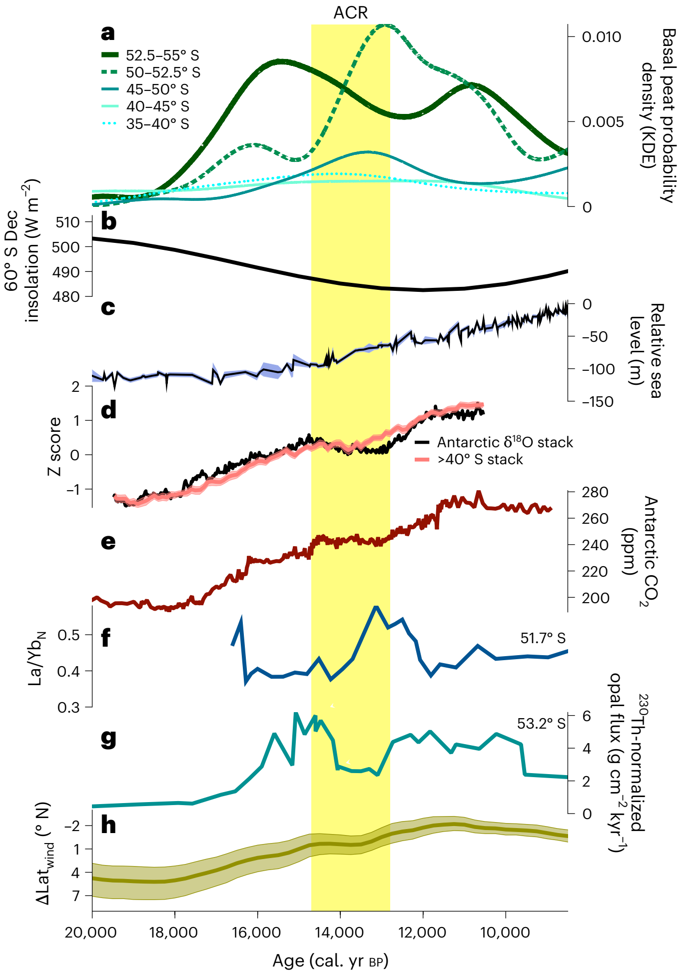

Fig. 3 | Peat initiation and climate proxies through the last glacial. a, KDE of peat initiation for different latitude bands. **b**, 60° S December (Dec) insolation[66]. **c**, Relative sea-level curve[40] (shading represents the 95% probability limiting values). **d**, *Z*-score of Antarctic $\delta^{18}O$ stack and Southern Ocean and terrestrial temperature records from south of 40° S (shading represents the standard error of the mean of the proxy stack)[41]. **e**, CO_2 records from WAIS Divide[65]. **f**, La/Yb (*N*, upper continental crust-normalised) (distal dust) from the Hookers Point record, Falkland Islands (site latitude 51.7° S)[42]. **g**, Atlantic opal flux (a proxy for upwelling south of the Antarctic Polar Front), showing a decrease in the opal flux during the ACR (site latitude 53.2° S)[32]. **h**, Reconstructed zonal-mean wind latitude (ΔLat_{wind}) (with shading representing the 95th percentile)[46]. The yellow shaded bar indicates the ACR (14,700–12,800 cal. yr BP)[41].

attempt to constrain the precise width of the wind belt; instead we demonstrate that SWW shifts are detectable at spatial scales of at least 2.5° of latitude.

This interpretation of the latitudinal phasing of peat initiation driven by changes in the SWW is further supported by multiple proxy records from the southern mid-latitudes. For instance, reconstructions of biogenic opal burial from the South Atlantic (53.2° S) show distinct periods of enhanced upwelling immediately before and after the ACR (Fig. 3g), coinciding with rising atmospheric CO_2 during the last deglaciation[32]. Despite age uncertainties, it seems likely that these two periods of upwelling correspond with the two peaks of peat initiation across the 52.5–55° S latitude band on either side of the ACR, both driven by the poleward-shifted SWW. This interpretation is reinforced by a compilation of planktic foraminiferal $\delta^{18}O$ records from across the Southern Ocean, where sea surface temperature fronts suggest a >5° poleward shift in the wind belt during deglaciation, a pattern closely tracking the evolution of atmospheric CO_2 (Fig. 3h)[46]. A small equatorward shift in wind latitude during the ACR aligns with transient Southern Hemisphere cooling, suggesting modulation of SWW behaviour that influenced the phasing of peat initiation across the region. Collectively, these studies support our interpretations that before the ACR, the westerlies had a core latitude around 52.5–55° S, which shifted northwards by a few degrees to ~50–52.5° S during the ACR and returned southwards thereafter.

Terrestrial records show similar patterns. In the southernmost latitudinal band in the Pacific sector, pollen- and spore-based transfer functions used to derive temperature estimates from Campbell Island (52.5° S) suggest peak wind intensity in the early Holocene, consistent with a northward SWW displacement during the ACR[8], as well as a rapid warming from 12,000 to 10,000 cal. yr BP. High wind velocities are also inferred from sea-salt aerosols and minerogenic particles accumulating in lake sediments on Macquarie Island (54° S) from 12,000 to 11,000 cal. yr BP[18]. This combination of strengthened SWW and rising temperatures probably contributed to the second peak in peat-forming sites at around 11,000 cal. yr BP.

Farther north, long-distance pollen types *Nothofagus* and *Maytenus* first appear in a Falkland Islands peat sequence (51.7° S) during the ACR, indicating the greater influence of the westerly winds in the 50–52.5° S band[47]. Higher moisture availability is also inferred, with the absence of woody macrofossils indicating that conditions were too wet for the establishment of heathlands. A La/Yb (distal dust) record from the Falkland Islands[42] shows peak dust fluxes at ~13,000 cal. yr BP (Fig. 3f), closely matching the timing of peat initiation in this latitudinal band. Concurrently, enhanced water availability (determined from the $\delta^{13}C$ of *n*-alkane C_{29} from plant waxes preserved in tarn sediments) further supports an increased SWW influence at this time[48]. In Patagonia, increases in cold-tolerant species and glacial advances at these latitudes suggest a cold/wet climate during the ACR consistent with increased SWW influence[33,49,50]. Similarly, in the Pacific sector, records from Western Tasmania and New Zealand at the northern edge of the contemporary SWW belt (40–44° S), also indicate an increased influence of the SWW during the early ACR, shown by reduced biomass burning linked to wetter conditions[2] and glacial advances[51].

During the early Holocene, lake sediment records indicate high precipitation and elevated temperatures in southern South America, probably promoting peat growth[20]. The early Holocene thermal maxima may have contributed to the KDE peak in peat initiation at 8,000 cal. yr BP, although sparse temperature records from the region limit precise estimates of warming[29,52]. While warmer and moister conditions (linked to a strengthening of the SWW) have been reported between 5,000 and 2,000 cal. yr BP[11], they did not translate to new areas of peat formation, probably because most suitable sites were already colonized. Over the past two millennia, renewed intensification of the SWW in the southwest Pacific[16], along with a stronger Amundsen Sea Low[11], may have facilitated peat establishment in previously uncolonized sites around 50° S.

SWW as a driver of ocean–atmosphere carbon exchange

Our study reveals distinct latitudinal patterns in the initiation of southern extratropical peatlands during the deglaciation, driven primarily by shifts in the strength and position of the SWW. While local factors, such as geomorphology and glacial history, can influence peat formation, the broader spatial patterns align most closely with SWW variations. Stronger westerlies enhance precipitation, regulate evaporation and transport nutrients, all of which create favourable conditions for the establishment of peatlands. The dataset of peat initiation ages compiled here provides a spatially coherent record of SWW shifts during a critical period of limited climate and environmental records. Crucially, these shifts align with millennial-scale CO_2 variations, supporting the hypothesis that the SWW played a key role in regulating atmospheric CO_2 during the deglaciation[32,53].

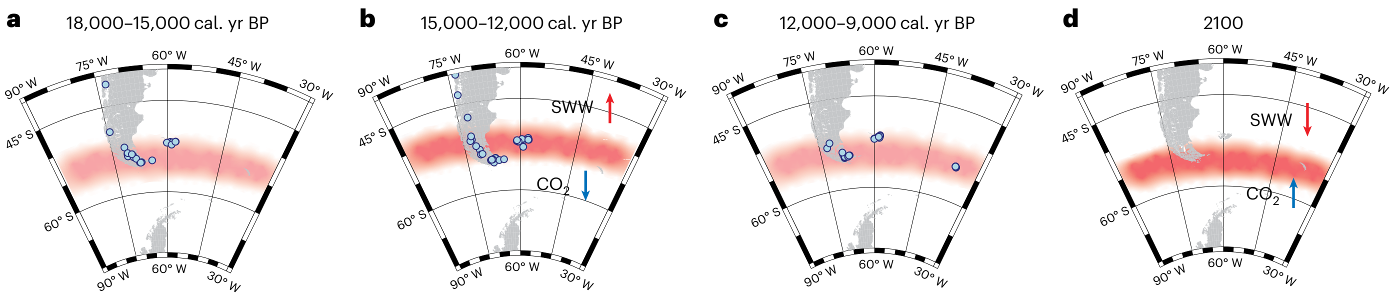

Fig. 4 | Past and future shifts in the SWW. a–**c**, Schematics showing the suggested shifts of the core SWW (red) in the South Atlantic during the last deglaciation from 18,000–15,000 cal. yr BP (**a**), 15,000–12,000 cal. yr BP (**b**) and 12,000–9,000 cal. yr BP (**c**) and projected changes for 2100 based on the Coupled Model Intercomparison Project Phase 6 multimodel mean under representative concentration pathway 8.5 (**d**)[67]. Blue dots indicate the locations of peat initiation between the time periods indicated. Stronger winds are represented by more intense red shading.

Since the mid- to late twentieth century, a strengthening and poleward shift of the SWW has been observed[54], along with accelerated warming in the South Atlantic[55], Southern Indian Ocean[56] and southwest Pacific[57]. This trend is anomalous within the past millennium[58], and has been associated with changes in climate, air–sea carbon fluxes, sea-ice trends and ice sheet dynamics on interannual to multidecadal timescales[3,59–62]. Model projections suggest that SWW intensification will continue under future warming scenarios (Fig. 4d), raising concerns about increased outgassing of natural CO_2 from the Southern Ocean[46,63]. Our findings reinforce the role of the SWW in modulating the ocean–atmosphere carbon flux, and suggest that this feedback is likely to become increasingly important in the future.

Online content

Any methods, additional references, Nature Portfolio reporting summaries, source data, extended data, supplementary information, acknowledgements, peer review information; details of author contributions and competing interests; and statements of data and code availability are available at https://doi.org/10.1038/s41561-025-01842-w.

References

1. Chemke, R., Ming, Y. & Yuval, J. The intensification of winter mid-latitude storm tracks in the Southern Hemisphere. *Nat. Clim. Change* **12**, 553–557 (2022).
2. Fletcher, M.-S. et al. Northward shift of the southern westerlies during the Antarctic Cold Reversal. *Quat. Sci. Rev.* **271**, 107189 (2021).
3. Landschützer, P. et al. The reinvigoration of the Southern Ocean carbon sink. *Science* **349**, 1221–1224 (2015).
4. Moreno, P. I. et al. Onset and evolution of Southern Annular Mode-like changes at centennial timescale. *Sci. Rep.* **8**, 3458 (2018).
5. Gillett, N. P., Kell, T. D. & Jones, P. D. Regional climate impacts of the Southern Annular Mode. *Geophys. Res. Lett.* **33**, L23704 (2006).
6. Goyal, R., Sen Gupta, A., Jucker, M. & England, M. H. Historical and projected changes in the Southern Hemisphere surface westerlies. *Geophys. Res. Lett.* **48**, e2020GL090849 (2021).
7. PAGES 2k Consortium. Continental-scale temperature variability during the past two millennia. *Nat. Geosci.* **6**, 339–346 (2013).
8. McGlone, M. S., Turney, C. S. M., Wilmshurst, J. M., Renwick, J. & Pahnke, K. Divergent trends in land and ocean temperature in the Southern Ocean over the past 18,000 years. *Nat. Geosci.* **3**, 622–626 (2010).
9. León, C. A. et al. Peatlands of southern South America: a review. *Mires Peat* https://doi.org/10.19189/MaP.2020 (2021).
10. Van Der Putten, N. et al. Peat bank growth, Holocene palaeoecology and climate history of South Georgia (sub-Antarctica), based on a botanical macrofossil record. *Quat. Sci. Rev.* **28**, 65–79 (2009).
11. Thomas, Z. A. et al. Evidence for increased expression of the Amundsen Sea Low over the South Atlantic during the late Holocene. *Clim. Past* **14**, 1727–1738 (2018).
12. Convey, P. in *Encyclopedia of the World's Biomes* (eds Goldstein, M. I. & DellaSala, D. A.) 666–685 (Elsevier, 2020).
13. Tamhane, J. et al. Mid-Holocene intensification of Southern Hemisphere westerly winds and implications for regional climate dynamics. *Quat. Sci. Rev.* **305**, 108007 (2023).
14. Zwier, M., Van Der Bilt, W. G., De Stigter, H. & Bjune, A. E. Pollen evidence of variations in Holocene climate and Southern Hemisphere westerly wind strength on sub-Antarctic South Georgia. *Holocene* **32**, 147–158 (2022).
15. Turney, C. S. M. et al. Reconstructing atmospheric circulation over southern New Zealand: establishment of modern westerly airflow 5500 years ago and implications for Southern Hemisphere Holocene climate change. *Quat. Sci. Rev.* **159**, 77–87 (2017).
16. Turney, C. S. M. et al. Intensification of Southern Hemisphere westerly winds 2000-1000 years ago: evidence from the subantarctic Campbell and Auckland Islands (52-50°S). *J. Quat. Sci.* **31**, 12–19 (2016).
17. Turney, C. S. M. et al. A 250-year periodicity in Southern Hemisphere westerly winds over the last 2600 years. *Clim. Past* **12**, 189–200 (2016).
18. Saunders, K. M. et al. Holocene dynamics of the Southern Hemisphere westerly winds and possible links to CO_2 outgassing. *Nat. Geosci.* **11**, 650–655 (2018).
19. Koffman, B. G. et al. Centennial-scale variability of the Southern Hemisphere westerly wind belt in the eastern Pacific over the past two millennia. *Clim. Past* **10**, 1125–1144 (2014).
20. Lamy, F. et al. Holocene changes in the position and intensity of the southern westerly wind belt. *Nat. Geosci.* **3**, 695–699 (2010).
21. Browne, I. M. et al. Late Holocene intensification of the westerly winds at the subantarctic Auckland Islands (51° S), New Zealand. *Clim. Past* **13**, 1301–1322 (2017).
22. Pedro, J. B. et al. The last deglaciation: timing the bipolar seesaw. *Clim. Past* **7**, 671–683 (2011).
23. Rydin, H., Jeglum, J. K. & Bennett, K. D. *The Biology of Peatlands* 2nd edn (Oxford Univ. Press, 2013).
24. Müller, J. & Joos, F. Committed and projected future changes in global peatlands – continued transient model simulations since the Last Glacial Maximum. *Biogeosciences* **18**, 3657–3687 (2021).
25. Charman, D. J. et al. Drivers of Holocene peatland carbon accumulation across a climate gradient in northeastern North America. *Quat. Sci. Rev.* **121**, 110–119 (2015).
26. Treat, C. C. et al. Widespread global peatland establishment and persistence over the last 130,000 y. *Proc. Natl Acad. Sci. USA* **116**, 4822–4827 (2019).

27. Yu, Z., Loisel, J., Brosseau, D. P., Beilman, D. W. & Hunt, S. J. Global peatland dynamics since the Last Glacial Maximum. *Geophys. Res. Lett.* **37**, L13402 (2010).
28. Chaudhary, N., Miller, P. A. & Smith, B. Biotic and abiotic drivers of peatland growth and microtopography: a model demonstration. *Ecosystems* **21**, 1196–1214 (2018).
29. Morris, P. J. et al. Global peatland initiation driven by regionally asynchronous warming. *Proc. Natl Acad. Sci. USA* **115**, 4851–4856 (2018).
30. Thomas, Z. A. et al. Supplementary data and supplementary code—westerly wind shifts drove Southern Hemisphere mid-latitude peat growth during the last glacial, Thomas et al. *Zenodo* https://doi.org/10.5281/zenodo.17228226 (2025).
31. Hogg, A. G. et al. SHCal20 Southern Hemisphere Calibration, 0–55,000 years cal BP. *Radiocarbon* **62**, 759–778 (2020).
32. Anderson, R. F. et al. Wind-driven upwelling in the Southern Ocean and the deglacial rise in atmospheric CO_2. *Science* **323**, 1443–1448 (2009).
33. Davies, B. J. et al. The evolution of the Patagonian Ice Sheet from 35 ka to the present day (PATICE). *Earth Sci. Rev.* **204**, 103152 (2020).
34. Garreaud, R., Lopez, P., Minvielle, M. & Rojas, M. Large-scale control on the Patagonian climate. *J. Clim.* **26**, 215–230 (2013).
35. Garreaud, R. Precipitation and circulation covariability in the extratropics. *J. Clim.* **20**, 4789–4797 (2007).
36. Xia, Z., Oppedal, L. T., Van Der Putten, N., Bakke, J. & Yu, Z. Ecological response of a glacier-fed peatland to late Holocene climate and glacier changes on subantarctic South Georgia. *Quat. Sci. Rev.* **250**, 106679 (2020).
37. Nel, W., Hodgson, D. A., Hedding, D. W., Whittle, A. & Rudolph, E. M. Twenty-thousand-year gap between deglaciation and peat formation on sub-Antarctic Marion Island attributed to climate and sea level change. *J. Quat. Sci.* **40**, 437–444 (2025).
38. Kylander, M. E. et al. Mineral dust as a driver of carbon accumulation in northern latitudes. *Sci. Rep.* **8**, 6876 (2018).
39. Ratcliffe, J. L. et al. Rapid carbon accumulation in a peatland following Late Holocene tephra deposition, New Zealand. *Quat. Sci. Rev.* **246**, 106505 (2020).
40. Lambeck, K., Rouby, H., Purcell, A., Sun, Y. & Sambridge, M. Sea level and global ice volumes from the Last Glacial Maximum to the Holocene. *Proc. Natl Acad. Sci. USA* **111**, 15296–15303 (2014).
41. Pedro, J. B. et al. The spatial extent and dynamics of the Antarctic Cold Reversal. *Nat. Geosci.* **9**, 51–55 (2016).
42. Monteath, A. et al. Late glacial–Holocene record of Southern Hemisphere westerly wind dynamics from the Falkland Islands, South Atlantic Ocean. *Geology* **50**, 880–885 (2022).
43. Fletcher, M.-S. & Moreno, P. I. Zonally symmetric changes in the strength and position of the Southern Westerlies drove atmospheric CO_2 variations over the past 14 k.y. *Geology* **39**, 419–422 (2011).
44. Moreno, P. I. & Videla, J. Centennial and millennial-scale hydroclimate changes in northwestern Patagonia since 16,000 yr BP. *Quat. Sci. Rev.* **149**, 326–337 (2016).
45. Mariani, M. et al. Coupling of the Intertropical Convergence Zone and Southern Hemisphere mid-latitude climate during the early to mid-Holocene. *Geology* **45**, 1083–1086 (2017).
46. Gray, W. R. et al. Poleward shift in the Southern Hemisphere westerly winds synchronous with the deglacial rise in CO_2. *Paleoceanogr. Paleoclimatol.* **38**, e2023PA004666 (2023).
47. Scaife, R. G. et al. The Falkland Islands' palaeoecological response to millennial-scale climate perturbations during the Pleistocene–Holocene transition: implications for future vegetation stability in the southern ocean islands. *J. Quat. Sci.* **34**, 609–620 (2019).
48. Spoth, M. et al. Tracking the southern hemisphere westerlies during and since the last glacial maximum with multiproxy lake records from the Falkland Islands (52 °S). *Quat. Sci. Rev.* **311**, 108135 (2023).
49. Moreno, P. I. Timing and structure of vegetation, fire, and climate changes on the Pacific slope of northwestern Patagonia since the last glacial termination. *Quat. Sci. Rev.* **238**, 106328 (2020).
50. Moreno, P. I. et al. An early Holocene westerly minimum in the southern mid-latitudes. *Quat. Sci. Rev.* **251**, 106730 (2021).
51. Tielidze, L. G. et al. Early glacier advance in New Zealand during the Antarctic Cold Reversal. *J. Quat. Sci.* **38**, 544–562 (2023).
52. Cartapanis, O., Jonkers, L., Moffa-Sanchez, P., Jaccard, S. L. & de Vernal, A. Complex spatio-temporal structure of the Holocene Thermal Maximum. *Nat. Commun.* **13**, 5662 (2022).
53. Toggweiler, J. R., Russell, J. L. & Carson, S. R. Midlatitude westerlies, atmospheric CO_2, and climate change during the ice ages. *Paleoceanography* **21**, PA2005 (2006).
54. Visbeck, M. A station-based Southern Annular Mode index from 1884 to 2005. *J. Clim.* **22**, 940–950 (2009).
55. Thomas, Z. et al. A new daily observational record from Grytviken, South Georgia: exploring twentieth-century extremes in the South Atlantic. *J. Clim.* **31**, 1743–1755 (2018).
56. Nel, W., Hedding, D. W. & Rudolph, E. M. The sub-Antarctic islands are increasingly warming in the 21st century. *Antarct. Sci.* **35**, 124–126 (2023).
57. Caloiero, T. Trend of monthly temperature and daily extreme temperature during 1951–2012 in New Zealand. *Theor. Appl. Climatol.* **129**, 111–127 (2017).
58. Abram, N. J. et al. Evolution of the Southern Annular Mode during the past millennium. *Nat. Clim. Change* **4**, 564–569 (2014).
59. Le Quéré, C. et al. Saturation of the Southern Ocean CO_2 sink due to recent climate change. *Science* **316**, 1735–1738 (2007).
60. Pritchard, H. D. et al. Antarctic ice-sheet loss driven by basal melting of ice shelves. *Nature* **484**, 502–505 (2012).
61. Jones, J. M. et al. Assessing recent trends in high-latitude Southern Hemisphere surface climate. *Nat. Clim. Change* **6**, 917–926 (2016).
62. Schroeter, S., O'Kane, T. J. & Sandery, P. A. Antarctic sea ice regime shift associated with decreasing zonal symmetry in the Southern Annular Mode. *Cryosphere* **17**, 701–717 (2023).
63. Menviel, L. C. et al. Enhanced Southern Ocean CO_2 outgassing as a result of stronger and poleward shifted southern hemispheric westerlies. *Biogeosciences* **20**, 4413–4431 (2023).
64. Hersbach, H. et al. The ERA5 global reanalysis. *Q. J. R. Meteorol. Soc.* **146**, 1999–2049 (2020).
65. Marcott, S. A. et al. Centennial-scale changes in the global carbon cycle during the last deglaciation. *Nature* **514**, 616–619 (2014).
66. Laskar, J. et al. A long-term numerical solution for the insolation quantities of the Earth. *Astron. Astrophys.* **428**, 261–285 (2004).
67. Goyal, R., England, M. H., Jucker, M. & Sen Gupta, A. Response of Southern Hemisphere western boundary current regions to future zonally symmetric and asymmetric atmospheric changes. *J. Geophys. Res. Oceans* **126**, e2021JC017858 (2021).

Publisher's note Springer Nature remains neutral with regard to jurisdictional claims in published maps and institutional affiliations.

[1]School of Geography and Environmental Science, University of Southampton, Southampton, UK. [2]Centre of Excellence for Australian Biodiversity and Heritage, School of Science, University of Wollongong, Sydney, New South Wales, Australia. [3]School of Biological, Earth and Environmental Sciences, University of New South Wales, Sydney, New South Wales, Australia. [4]School of Energy, Geoscience, Infrastructure and Society, Heriot-Watt University, Edinburgh, UK. [5]Department of Anthropology and Archaeology, University of Bristol, Bristol, UK. [6]Linacre College, University of Oxford, Oxford, UK. [7]Department of Geography, University of Nevada, Reno, Reno, NV, USA. [8]Mark Wainwright Analytical Centre, University of New South Wales, Sydney, New South Wales, Australia. [9]Faculty of Science and Engineering, University of Plymouth, Plymouth, UK. [10]South Atlantic Environmental Research Institute (SAERI), Stanley, Falkland Islands. [11]UK Centre for Ecology and Hydrology, Bangor, UK. [12]School of Biological Sciences (Zoology), University of Aberdeen, Aberdeen, UK. ✉e-mail: z.thomas@soton.ac.uk

Methods

Falkland Islands basal peat dataset

Thirty sites were visited across the Falkland Islands in March 2020, and basal peat samples were collected (Supplementary Data 1, ref. 30). Cores were either extracted using a Russian D-section corer or, in areas where the bases of peat banks were exposed, the surface was cleaned and basal samples extracted with a spatula. All samples were radiocarbon dated at the Chronos Radiocarbon Facility at the University of New South Wales following the 'Peat/Sediments' protocol and targeting alkali insoluble fractions through acid–base–acid rinsing[68]. Although terrestrial macrofossils are generally considered to be the most reliable material for ^{14}C sample selection within a sediment matrix[69,70], no sufficiently large terrestrial macrofossils were identified in the basal peat samples. In the absence of terrestrial macrofossils, bulk peat was analysed, with care taken to remove any roots before chemical pretreatment. In samples with an abundance of root and rootlet material, a 250 µm sieve was used to separate this material to ensure the removal of possible contaminants. All radiocarbon ages were calibrated with SHCal20[31].

Studies have shown that subtle differences in the selection and treatment of basal peat ^{14}C ages can have important implications for the interpretation of trends in peatland initiation[71]. Here we used data that have a direct stratigraphic association between the basal ^{14}C age and peat initiation. Many ages presented here are from the bulk peat fraction: this would generally skew ages to be younger, rather than older (due to root penetration). Any 'contamination' from older carbon is unlikely as the basal age represents the initiation of organic matter deposition on a previously inorganic landscape, thus basal ages often reflect minimum ages for peatland initiation[72].

Southern mid-latitude basal peat dataset

A literature search was undertaken to identify published basal peat radiocarbon ages from sites south of 35° S (Supplementary Data 1, ref. 30). Data were taken from previous compilations[27,73], as well as original published sources. All dates (201) were recalibrated with SHCal20[31]. As discussed in Loisel et al.[74], the 'basal peat ages' can represent the initiation of organic matter accumulation, rather than the formation of peat per se. However, given that 'pre-peatland' ecosystems tend to exist only for a few hundred years[75], and that the climatic conditions necessary for their formation are similar, this distinction between peat and organic accumulation is unlikely to be significant. Another potentially important consideration is that basal peat ages are generally based on a single location, and do not take into account the differing lateral growth of peatlands. However, when we took samples close to sites used in previous studies[47,73], we found that the basal dates were remarkably consistent. This suggests that a single basal date should be broadly representative of the local area. Where sites (defined as distinct hydrological systems within a local area) have multiple basal dates, the oldest age was taken to represent the most useful measure of the timing of peat initiation for the purpose of this study. The total number of basal ages that we collated is 239, but removing sites with multiple basal ages to avoid biasing the analysis results in a total number of 201 used. The sample contexts of all sites were checked to ensure that the radiocarbon age represented the initiation of peat growth. Any radiocarbon ages that were not considered basal were removed from our analysis.

Kernel density estimate (KDE) modelling

To investigate temporal phases of peat formation, we incorporated the radiocarbon ages as a KDE model in OxCal, a program designed for the analysis of chronological information[76]. The kernel density is one of the most widely used non-parametric methods for estimating underlying distributions in radiocarbon data and is considered superior to a summed distribution because the KDE takes into account the uncertainty associated with radiocarbon calibration and allows for multimodality in the data. Careful consideration was given to the kernel choice and bandwidth estimation to ensure that the underlying distribution is not oversmoothed. The upper limit (as described by Silverman's rule; ref. 77) ensures an upper limit whereby kernels that would be wider than optimal are not considered. The KDE model uses the following parameters for all analysis: KDE_Model('Name', N(0,1),U(0,0.5)), where N is the kernel range to be used and U is the factor to be applied relative to Silverman's rule. Effectively, this kernel range allows the bandwidth to take any value, but with the upper limit defined by half of the Silverman estimate. This choice ensures that the KDE plot does not overfit the data (which is particularly important when the number of basal ages is small), effectively eliminating the high-frequency noise while retaining the lower-frequency signal[76].

To investigate the spatial phasing of peat initiation, the dataset was divided into different regions and latitudinal bands from which individual KDE models were run (Supplementary Fig. 1 and Supplementary Data 1). The size of each latitudinal band was determined by data availability, with bands set at either 5° or 2.5° when more than 30 basal peat ages were available to generate a robust KDE. The numbers of sites in each latitudinal band and sector are listed in Supplementary Table 1.

Ethics statement. We affirm that all geological materials sampled were collected and exported in a responsible manner and in accordance with relevant permits and local laws.

Data availability

The data supporting the findings of this study are available within the Article and Supplementary Information and via Zenodo at https://doi.org/10.5281/zenodo.17228226 (ref. 30). The radiocarbon ages produced and published ages used in this study are available in Supplementary Data 1. Source data for Figs. 2 and 3a are available in Supplementary Data 1. The base maps in Figs. 1 and 4 and Supplementary Figs. 2–7 were produced using Generic Mapping Tools v6[78].

Code availability

The OxCal codes associated with this study are available in Supplementary Code 1 and via Zenodo at https://doi.org/10.5281/zenodo.17228226 (ref. 30).

References

68. Turney, C. et al. Radiocarbon protocols and first intercomparison results from the Chronos ^{14}Carbon-Cycle Facility, University of New South Wales, Sydney, Australia. *Radiocarbon* **63**, 1003–1023 (2021).
69. Thomas, Z. A., Turney, C. S. M., Hogg, A., Williams, A. N. & Fogwill, C. J. Investigating subantarctic ^{14}C ages of different peat components: site and sample selection for developing robust age models in dynamic landscapes. *Radiocarbon* **61**, 1009–1027 (2019).
70. Blockley, S. P. E. et al. Synchronisation of palaeoenvironmental records over the last 60,000 years, and an extended INTIMATE event stratigraphy to 48,000 b2k. *Quat. Sci. Rev.* **36**, 2–10 (2012).
71. Quik, C. et al. Dating basal peat: the geochronology of peat initiation revisited. *Quat. Geochronol.* **72**, 101278 (2022).
72. Reyes, A. V. & Cooke, C. A. Northern peatland initiation lagged abrupt increases in deglacial atmospheric CH_4. *Proc. Natl Acad. Sci. USA* **108**, 4748–4753 (2011).
73. Payne, R. J. et al. Peatland initiation and carbon accumulation in the Falkland Islands. *Quat. Sci. Rev.* **212**, 213–218 (2019).
74. Loisel, J., Garneau, M. & Hélie, J.-F. Modern sphagnum $\delta^{13}C$ signatures follow a surface moisture gradient in two boreal peat bogs, James Bay lowlands, Québec. *J. Quat. Sci.* **24**, 209–214 (2009).
75. Jones, M. C., Peteet, D. M., Kurdyla, D. & Guilderson, T. Climate and vegetation history from a 14,000-year peatland record, Kenai Peninsula, Alaska. *Quat. Res.* **72**, 207–217 (2009).

76. Bronk Ramsey, C. Methods for summarizing radiocarbon datasets. *Radiocarbon* **59**, 1809–1833 (2017).
77. Silverman, B. W. *Density Estimation for Statistics and Data Analysis* (Chapman & Hall/CRC, 1998).
78. Wessel, P. et al. The Generic Mapping Tools version 6. *Geochem. Geophys. Geosyst.* **20**, 5556–5564 (2019).

Acknowledgements

Z.A.T. received funding from an Australian Research Council Fellowship (DE200100907) and UKRI Future Leaders Fellowship (MR/Y016351/1). Special thanks go to the South Atlantic Environmental Research Institute (SAERI), and L. Summers in particular, for logistical help. We are grateful to the many landowners who kindly provided access permissions.

Author contributions

Z.A.T. conceived and coordinated the study, led fieldwork and laboratory analyses, analysed data, prepared figures and wrote the first manuscript draft. H.C., L.B.-V., H.A.H., C.T. and C.M. designed and conducted laboratory methodologies. S.C. and P.B. informed on sampling strategy and fieldwork logistics. H.C., C.T. and C.F. contributed to data interpretation and discussions of implications. All authors contributed to integrating the results, interpreting the findings and revising the manuscript.

Competing interests

The authors declare no competing interests.

Additional information

Supplementary information The online version contains supplementary material available at https://doi.org/10.1038/s41561-025-01842-w.

Correspondence and requests for materials should be addressed to Zoë A. Thomas.

Peer review information *Nature Geoscience* thanks David Hedding and the other, anonymous, reviewer(s) for their contribution to the peer review of this work. Primary Handling Editor: James Super, in collaboration with the *Nature Geoscience* team.